TECHNISCHE MECHANIK
European Journal of Engineering Mechanics
Diamond Open Access
journal homepage: www.ovgu.de/techmech

Tech. Mech., Vol. 46, Is. 1, (2026), 12–24
Received: 06.11.2025
Accepted: 09.02.2026
Available online: 16.02.2026

Numerical investigation of a lifted methane/air jet flame using stochastic map-based turbulence modeling

Tommy Starick[1]* and Heiko Schmidt[1,2]

[1] Brandenburg University of Technology (BTU) Cottbus-Senftenberg, Institute of Transport Technology, Chair of Numerical Fluid and Gas Dynamics, Siemens-Halske-Ring 15a, 03046 Cottbus, Germany.
[2] Brandenburg University of Technology (BTU) Cottbus-Senftenberg, Energy Innovation Center (EIZ), Scientific Computing Lab (SCL), 03046 Cottbus, Germany.

Abstract: Turbulent combustion processes are ubiquitous phenomena and play a fundamental role in a wide range of industrial applications, transportation, and energy production. The accurate numerical investigation of turbulent reacting flows is particularly challenging owing to the wide range of spatial and temporal scales involved. Here, the nonpremixed chemically reacting flow of a lifted methane/air jet flame in a vitiated coflow is studied using the map-based stochastic one-dimensional turbulence (ODT) model. The ODT model is efficient in terms of computational costs and provides nonetheless full-scale resolution along a notional line of sight crossing the turbulent reactive flow field. ODT uses a stochastic formulation for the turbulent advection and considers diffusion and reaction effects along the one-dimensional domain by temporally advancing deterministic evolution equations. In the considered Cabra burner configuration [Combust. Flame 143 491-506 (2005)], a jet flame issues from a central nozzle into a vitiated coflow of hot reaction products generated from an array of lean hydrogen/air flames. For the representation of the methane/air combustion, a reduced and detailed reaction mechanism with 19 and 53 species is used, respectively. The centerline profiles for mixture fraction, temperature and species mass fractions reveal reasonable agreement with the experimental measurements. Scatter plots and two-dimensional visualizations of the jet flame are also given including an assessment of an autoignition index used to differentiate between autoignition-driven and flame-propagation-dominated reaction zones. A parametric study is performed to examine the sensitivity of the flame to variations in jet velocity, coflow velocity, and coflow temperature. The results highlight the critical role of the interaction between the hot vitiated coflow and the cold unburnt jet in governing ignition, stabilization, and overall reaction dynamics. Despite its reduced-order formulation, the ODT model captures the essential physics of turbulent nonpremixed combustion and provides predictions that compare favorably with experimental observations at a significantly reduced computational cost.

Keywords: autoignition, lifted jet flame, methane/air combustion, ODT, one-dimensional turbulence, stochastic turbulence modeling

1 Introduction

Recirculation burners are widely used in industry and face increasingly stringent demands for reduced pollutant emissions, higher efficiency, and broader fuel and operational flexibility. The numerical investigation of these burners is challenging due to the recirculation of hot combustion products. Vitiated coflow burners instead consist of a lifted jet flame in an environment of hot combustion products and exhibit similar characteristics for chemical kinetics, heat transfer and molecular transport as recirculation burners, while avoiding their complex recirculating fluid mechanics, as detailed in Cabra et al. (2005).

Despite the simplified representation of a recirculation burner as a vitiated coflow burner, accurately capturing turbulent reactive flows remains a significant challenge in numerical fluid dynamics. In particular, the subtle molecular processes underlying chemical reactions require resolution of all relevant spatial and temporal scales to accurately capture the state-space statistics. Direct numerical simulation (DNS) would be the ideal tool to numerically investigate turbulent flows due to the full resolution in combination with the absence of modeling errors. However, for most industrially relevant applications, DNS is computationally prohibitive and therefore not feasible at present or in the foreseeable future (Domingo and Vervisch, 2023). In addition, the computational effort increases drastically when detailed chemical reaction mechanisms are taken into account.

To enable numerical investigation of turbulent reactive flows, turbulence closure models are commonly employed. In contrast to the full resolution provided by DNS, large-eddy simulation (LES) and Reynolds-averaged Navier–Stokes (RANS) approaches resolve the flow only in a filtered or averaged sense, thereby reducing the computational cost to practical levels. In order to remedy the lack of proper state-space information of the scalar composition in these lower-fidelity models, transported probability density function (PDF) methods are often employed (Pope, 1985).

The Cabra burner configuration (Cabra et al., 2002, 2005), which consists of a cold jet issuing from a central nozzle into a vitiated coflow of hot combustion products, represents an attractive test case since the subtle interactions between the hot coflow and the cold unburnt jet are crucial for ignition and flame stabilization. For this reason, the configuration has been extensively investigated

* E-mail address: Tommy.Starick@b-tu.de
doi: 10.24352/UB.OVGU-2026-003

using LES (Schulz et al., 2017; Zhang et al., 2018; Domingo et al., 2008; Ihme and See, 2010) and RANS (Cabra et al., 2005; Michel et al., 2009; Gkagkas and Lindstedt, 2007; Gordon et al., 2007) approaches. These studies show that averaged quantities are generally in reasonable agreement with experimental measurements and that the key combustion characteristics can be reproduced. Nevertheless, despite the use of filtering or averaging, LES and RANS simulations remain computationally intensive due to the resolution of detailed chemistry in combination with transported PDF methods. Consequently, their application is limited for extensive sensitivity analyses or parametric studies.

Reduced-order turbulence and mixing models provide an alternative approach. These models achieve a significant reduction in computational cost compared to DNS while preserving fundamental physical conservation principles and reproducing key features of turbulent flow phenomenology.

In reduced-order, map-based stochastic mixing and turbulence models, map-based transformations are applied in one-dimensional domains to mimic the effects of turbulent mixing and advection. Prominent examples include the linear eddy model (LEM) (Kerstein, 1988), which is a mixing model, and the one-dimensional turbulence (ODT) model (Kerstein, 1999), both formulated by A. Kerstein. The efficient utilization of currently available computational resources through dimensional order reduction, combined with full resolution of the entire range of scales along the one-dimensional domain, makes LEM and ODT particularly attractive for applications in which the small scales exhibit complex interactions of advection, diffusion and reaction.

Resolution of all time scales is incorporated in the model by construction, based on the calculated rate of implementation of eddy events, which is fixed in LEM and variable in ODT. Additionally, LEM and ODT allow a direct representation of the numerical solution in physical space, in contrast to the state-space representation obtained from PDF transport methods.

LEM has been successfully applied to a wide range of applications, including jets (Kerstein, 1990), multi-stream mixing (Kerstein, 1992; Sannan et al., 2013), and combustion (Kerstein, 1992; Lackmann et al., 2018; Oevermann et al., 2008). A key limitation of LEM arises from the fixed rate of eddy event implementation. In contrast, the stochastic sampling of eddy events in ODT depends on the instantaneous flow state. This modeling approach offers decisive advantages, such as the consideration of variable advection time scales, the coexistence of turbulent and non-turbulent regions, and the representation of small-scale features. For these reasons, ODT has been applied to a variety of turbulent reactive flows, including jet flames (Echekki et al., 2001; Ricks et al., 2010), cold jets (Lignell et al., 2018; Sharma et al., 2022), and constant-volume autoignition (Medina M. et al., 2018).

The main objective of this work is a scale-resolving and physics-based, yet computationally efficient, numerical investigation of a lifted methane/air jet flame in a vitiated coflow. The ODT results are comprehensively compared with the experimental measurements of Cabra et al. (2005). Additionally, an evaluation of the autoignition index is performed, and the sensitivity of the flame to variations in jet velocity, coflow velocity, and coflow temperature is investigated.

This paper is organized as follows. In Section 2, the ODT model formulation is discussed in more detail. Section 3 describes the flow configuration of the methane/air jet flame in a vitiated coflow considered in this study. In Section 4, the model results are presented and discussed. Finally, concluding remarks are provided.

2 ODT model formulation

The ODT model offers a significantly reduced numerical framework compared to DNS and LES, enabling full-scale resolution in the radial direction of the jet. This makes ODT an ideal tool for the numerical study of a lifted methane/air jet flame in a vitiated coflow. For this round jet flame, a cylindrical ODT formulation is used to account for the geometric proportions. This formulation is detailed in Lignell et al. (2018).

ODT employs a stochastic, map-based approach to represent turbulent advection. The diffusion and reaction kinetics along the one-dimensional domain are modeled through the temporal advancement of deterministic evolution equations. Unlike averaged or filtered simulation approaches, such as RANS or LES, ODT integrates molecular processes (e.g., chemical reactions and diffusive transport) without introducing additional approximations or modeling assumptions.

The effects of three-dimensional turbulence are incorporated into ODT through the use of stochastic *eddy events*. These eddy events directly represent the turbulent transport characteristics affecting fluid properties along the simulated one-dimensional domain. Each eddy event modifies property fields by applying a *triplet map*.

A triplet map is a measure-preserving transformation rule that ensures the continuity of advected fields, leading to the steepening of local property gradients (Lignell et al., 2018; Ashurst and Kerstein, 2005). The map operates by taking a line segment $[r_0, r_0 + l]$ with a randomly selected eddy location r_0 and size l, shrinking it to a third of its original length, and then placing three copies of the segment on the original domain. The middle copy is reversed. The features of the triplet map in the cylindrical ODT formulation can be reviewed in Lignell et al. (2018).

Eddy events are sampled in time using a marked Poisson process, with assumed Probability Density Functions (PDFs) for eddy locations r_0 and sizes l. This process replicates the statistics of turbulent flows on average by oversampling the number of events representing turbulent transport, while maintaining a target mean acceptance probability for the eddy events, as discussed in McDermott (2005) and Lignell et al. (2018). The acceptance probability of a particular eddy within a given sampling time interval Δt_{sample} is determined by calculating a rate λ of the eddy candidate.

The eddy rate λ, as shown in Eq. 1, depends on r_0, l, and the eddy event time scale τ. The time scale τ is proportional to the difference between the available kinetic energy E_{kin} in the eddy range and an energetic viscous penalty E_{vp} for suppressing excessively small eddies, as described in Lignell et al. (2018). While the energetic viscous penalty does not significantly affect the statistical results, it is beneficial for improving the model's performance.

$$\lambda(r_0, l, \tau) \equiv \frac{C}{l^2 \tau} \sim C\left(E_{kin} - Z E_{vp}\right) \tag{1}$$

C and Z are dimensionless ODT model parameters that are initially calibrated and then remain constant.
Due to its reduced dimensionality, ODT does not capture large-scale coherent structures. Occasionally, during the initial phase, the eddy sampling process may accept unphysically large eddies, which can negatively impact turbulent transport. To prevent this, ODT employs a large eddy suppression mechanism.
This mechanism eliminates eddies whose event time scale is disproportionately larger than the elapsed simulation time t. In general, eddies are only implemented if the following condition

$$\tau \leq \beta t \tag{2}$$

is satisfied, where β is another dimensionless ODT model parameter which is determined beforehand (Lignell et al., 2018).
Eddies are sampled sequentially in time. Once an eddy is implemented, a deterministic catch-up process takes place, advancing the diffusive-reactive transport equations up to the physical time at which the eddy was selected for implementation.
In an open system configuration, such as the lifted jet flame examined in this study, the deterministic evolution follows integral conservation laws based on a Lagrangian ODT formulation, as described in Lignell et al. (2018).
The integral expressions for the conservation of mass, momentum, and energy are presented below. The mass conservation equation is given as follows.

$$\frac{\mathrm{d}}{\mathrm{d}t}\int \rho r \mathrm{d}r = 0 \tag{3}$$

Here, ρ represents the density of the gas mixture, which is determined by its pressure, temperature, and molecular weight, as described by the ideal gas law.

$$P = \rho R_u T \sum_k \frac{Y_k}{M_k} \tag{4}$$

In this equation, P represents the thermodynamic pressure, which remains constant over time and space in the open jet flame configuration. Additionally, R_u denotes the universal gas constant, T is the temperature of the gas mixture, and Y_k and M_k correspond to the mass fractions and molecular weights of the k-th species that make up the gas mixture, respectively. The species conservation equation is given by following equation.

$$\frac{\mathrm{d}}{\mathrm{d}t}\int \rho Y_k r \mathrm{d}r = -\int \frac{1}{r}\frac{\partial}{\partial r}\left(r\rho V_k Y_k\right) r\mathrm{d}r \quad + \int \dot{w}_k r \mathrm{d}r \tag{5}$$

Here, V_k represents the species diffusion velocities, which require the same modeling approximations as those used in reactive DNS. Similarly, $\dot{w}_k$ denotes the species reaction rates, which are determined by an imported reaction mechanism under specified thermodynamic conditions.
For momentum conservation, we assume that radial transport is dominant and model the diffusion of momentum using the gradient of scalar-modeled shear stresses, following the approach described in Lignell et al. (2018).

$$\frac{\mathrm{d}}{\mathrm{d}t}\int \rho u_i r \mathrm{d}r = \int \frac{1}{r}\frac{\partial}{\partial r}\left(r\mu\frac{\partial u_i}{\partial r}\right) r\mathrm{d}r \tag{6}$$

In the momentum conservation equation, u_i stands for the three velocity components in the cylindrical system and μ is the dynamic viscosity of the gas mixture. Finally, the energy conservation in the open system is being represented by the conservation of enthalpy h in a zero Mach number limit approximation.

$$\frac{\mathrm{d}}{\mathrm{d}t}\int \rho h r \mathrm{d}r = -\int \frac{1}{r}\frac{\partial}{\partial r}\left(r\rho V_k Y_k h_k\right) r\mathrm{d}r \quad + \int \frac{1}{r}\frac{\partial}{\partial r}\left(r\lambda_t\frac{\partial T}{\partial r}\right) r\mathrm{d}r \tag{7}$$

In this equation, h_k stands for the sensible enthalpy of each k-th species and λ_t is the thermal conductivity of the mixture.
The deterministic time advancement of Eq. 3-7 is achieved using a finite volume method (FVM) with first-order time integration. For the analyzed lifted methane/air jet flame, an implicit time integration of Eq. 3-7 is applied, where the diffusive flux terms, calculated at the start of each time step, are treated as constants. This approach helps to mitigate the potentially restrictive CFL condition caused by stiff chemistry arising from the species chemical reaction source term. However, this converts the time integration in Eq. 6-7 into an explicit Euler method.
The density, which is updated after time-stepping the enthalpy and species conservation equations (Eq. 7 and 5), is computed using Eq. 4 based on the new mixture composition and temperature. Once the density is updated, mass conservation is enforced through a conservative remeshing of the grid, following the application of the mass conservation equation (Lignell et al., 2013). The fluid thermophysical properties are determined using the Cantera software suite (version 2.6.0), as described in Goodwin (2002).

3 Flow configuration

The Cabra burner configuration considered in this study (Cabra et al., 2005) consists of a lifted methane/air jet flame in a vitiated coflow, as schematically illustrated in Figure 1. The vitiated coflow, composed of hot combustion products, is generated from an array of lean H_2/air flames ($\phi = 0.4$). This coflow provides a preheated and partially burned environment into which the methane/air jet is injected, enabling the study of flame lift-off and stabilization under realistic conditions. The black line labeled $z/D = 0$ defines the reference axial location from which the ODT simulations are initiated.

According to Cabra et al. (2005), the temperature and species concentrations in the coflow can be considered spatially uniform across the domain of interest. Moreover, the flow field of the lifted jet is largely unaffected by interaction with ambient air, allowing the ODT simulations to neglect entrainment of surrounding air. Consequently, the coflow is initialized as a uniform stream in all simulations, creating a pure two-stream configuration that simplifies the modeling while retaining the essential physics of the lifted flame. In analogy with the experimental setup, the ODT domain size was set to match the coflow array, which has a diameter of 210 mm.

For the base case configuration, the coflow is initialized with a uniform velocity of 5.4 m/s, an atmospheric pressure of 1 atm, and a constant temperature of 1350 K. The corresponding composition and diameter of the coflow are summarized in Table 1. These conditions ensure that the jet interacts with a well-defined, preheated environment, facilitating the numerical investigation of flame lift-off, stabilization, and the effects of turbulence on the flame structure. By maintaining uniform coflow properties and excluding ambient air, the simulations isolate the key physical processes driving the lifted flame behavior, while minimizing numerical complexity and computational cost.

Tab. 1: Initial conditions for the jet and coflow are listed. X, mole fraction; u, velocity; T, temperature; D, diameter;

-	Jet	Coflow
D (mm)	4.57	210
u (m/s)	100	5.4
T (K)	320	1350
X_{CH_4}	0.33	0.0003
X_{O_2}	0.15	0.12
X_{N_2}	0.52	0.73
X_{H_2O}	0.0029	0.15
X_{OH} (ppm)	0.0	200
X_{H_2} (ppm)	100	100

The cold jet with a volumetric fuel mixture of 33% CH_4 and 67% air issues from a central nozzle into the vitiated coflow, as can be seen in Figure 1. The diameter D and composition of the jet are given in Table 1. The jet maintains a constant temperature of 320 K. For every single ODT realization, an instantaneous velocity profile is used generated by ODT pipe flow simulations with a fixed bulk velocity of 100 m/s. Consequently, the initial number of ODT grid cells for the jet is determined by the resolution of the underlying pipe flow simulation to ensure that the relevant turbulent and reactive scales at the inflow are captured. For the coflow, a relatively coarse initial grid is used, reflecting its uniform initialization. The ODT formulation employed in this study is based on

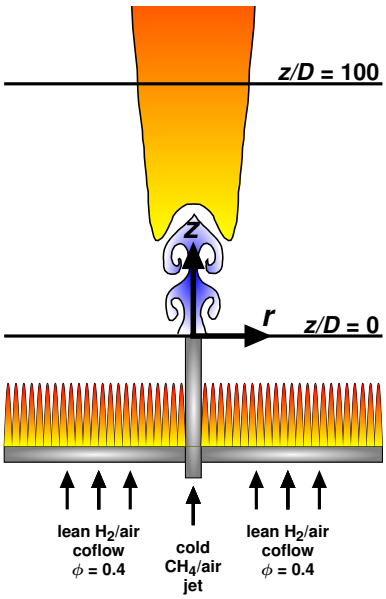

Fig. 1: Schematic illustration of the considered lifted methane/air jet flame in a vitiated coflow.

an adaptive grid Lignell et al. (2013), resulting in a variable number of grid cells throughout the simulation.

Chemical reactions and thermophysical properties are modeled using two approaches: (i) the detailed GRI-Mech 3.0 mechanism (Smith et al., 1999), comprising 53 species and 325 reactions, which captures the full chemical complexity of methane–air combustion, and (ii) a reduced mechanism (Lu and Law, 2008) with 19 species and 15 reactions, which provides a computationally efficient alternative while retaining the key combustion features.

The ODT results are compared with the stationary, spatially developing round jet flame measurements reported by Cabra et al. (2005). This comparison serves to validate the model and assess the abilities of ODT. However, the applied cylindrical ODT formulation only solves for a radial location r and time t. Consequently, a transformation between time and their corresponding downstream position z is required. This is implemented by a downstream advection of the ODT line with an instantaneous bulk velocity $\bar{u}$.

$$z(t) = z(t_0) + \int_{t_0}^{t} \bar{u}(t')dt' \tag{8}$$

Here, $z(t_0)$ marks the starting position. The bulk velocity $\bar{u}$ is calculated by the sum of the free-stream (coflow) velocity and the ratio of integrated momentum flux to integrated mass flux, as detailed in Echekki et al. (2001). In Figure 1, $z/D = 100$ illustrates symbolically a normalized downstream position of the ODT line of $z/D = 100$.

$$\bar{u}(t) = u_\infty + \left. \frac{\int_{-\infty}^{\infty} \rho(u-u_\infty)^2 r dr}{\int_{-\infty}^{\infty} \rho(u-u_\infty) r dr} \right|_t \tag{9}$$

For the definition of the mixture fraction, the commonly used Bilger's equation (Bilger et al., 1990) is applied.

$$f = \frac{2(Y_\mathrm{C} - Y_{\mathrm{C},2})/M_\mathrm{C} + (Y_\mathrm{H} - Y_{\mathrm{H},2})/2M_\mathrm{H} - (Y_\mathrm{O} - Y_{\mathrm{O},2})/M_\mathrm{O}}{2(Y_{\mathrm{C},1} - Y_{\mathrm{C},2})/M_\mathrm{C} + (Y_{\mathrm{H},1} - Y_{\mathrm{H},2})/2M_\mathrm{H} - (Y_{\mathrm{O},1} - Y_{\mathrm{O},2})/M_\mathrm{O}} \tag{10}$$

In this relation, M denotes the elemental masses and Y the mass fractions of carbon (C), hydrogen (H), and oxygen (O). The subscripts 1 and 2 mark the jet and the coflow, respectively.

4 Computational results

ODT simulations with a reduced and detailed mechanism were conducted and compared to the experimental measurements of Cabra et al. (2005). The Favre-averaged results are based on an ensemble of 1500 realizations, a number chosen to ensure statistically robust mean and fluctuation quantities. An initial investigation using a larger number of ensemble members showed no significant differences in the profiles. For all resented results, the ODT model parameters C and Z in Eq. 1 are set to $C = 18$ and $Z = 400$, consistent with the parameters employed in previous studies of a round jet flame using a cylindrical ODT formulation by Lignell et al. (2018). Large eddy suppression in the during the initial phase of the simulations is applied with a fixed model parameter parameter of $\beta = 1.17$.

4.1 Centerline profiles

Comparisons between experimental measurements of Cabra et al. (2005) and ODT simulations using both a reduced and a detailed reaction mechanism are presented in Figure 2. Centerline profiles of Favre-averaged species mass fractions $\tilde{Y}$, temperature $\tilde{T}$, mixture fraction $\tilde{f}$, and their corresponding fluctuations (T'', f'') are shown. In all plots, red and blue curves correspond to ODT results obtained with the reduced and detailed mechanisms, respectively, while the experimental data Cabra et al. (2005) are indicated by black circular markers.

The initial region up to $z/D \approx 40$ is dominated by non-reactive mixing of the cold jet with the hot coflow. In this phase, the centerline temperature rises gradually with low fluctuations, oxygen consumption is moderate, and the mixture fraction decreases strongly, accompanied by a peak in its fluctuations. Flame stabilization occurs at $z/D \approx 45$, where a sharp temperature increase, rapid oxygen depletion, hydroxyl radical formation, and a peak in temperature fluctuations are observed.

The ODT results for both reaction mechanisms are in reasonable agreement with the experimental data. This includes a correct representation of the mixing in the initial phase and an accurate capture of the combustion process, which is denoted by a rapid temperature rise and oxygen mass fraction drop. ODT also almost captures the trend and magnitude of the Favre fluctuations from the experimental measurements. It can be seen that the mean values of the mass fractions of O_2 and OH are slightly overpredicted for $z/D > 60$. The differences between both reaction mechanisms are negligible. The reduced mechanism of Lu and Law (2008), comprising 19 species and 15 reactions, is derived from a 30-species skeletal mechanism for methane–air combustion based on the detailed GRI-Mech 3.0 mechanism (Smith et al., 1999). For the investigated lifted methane/air jet flame, the reduced mechanism successfully preserves the essential characteristics of the full chemical kinetics, offering a computationally efficient alternative for simulation. Accordingly, the reduced mechanism was employed for the parametric studies on the sensitivity of the jet flame to temperature and velocity variations in Section 4.6, offering a computationally efficient approach while maintaining close agreement with the detailed mechanism.

4.2 Radial profiles

In addition to the centerline profiles, Fig. 3 presents radial profiles of the Favre-averaged temperature, Favre-averaged mixture fraction, and their corresponding fluctuations at selected downstream positions. As in the centerline plots, the red and blue curves represent ODT results obtained using a detailed and a reduced reaction mechanism, respectively. Experimental measurements are shown as black markers, with circular symbols denoting Favre-averaged values and square symbols indicating the corresponding fluctuations. These radial profiles provide insight into the spatial distribution of scalars across the jet.

In the upstream region $z/D = 15$ and $z/D = 30$, the flow is dominated by non-reactive mixing between the cold jet and the surrounding hot coflow. In this region, ODT reproduces the mean values and fluctuations of temperature and mixture fraction reasonably well, although minor deviations from the experimental measurements are evident. Nevertheless, where turbulent mixing predominates over chemical reaction, ODT reliably captures the evolution of scalar fields, including the gradual growth of temperature fluctuations and the reduction of mixture fraction due to entrainment, diffusion, and the progressive mixing of the cold jet with the hot coflow.

Further downstream, at $z/D = 50$ and $z/D = 70$, discrepancies between ODT predictions and experimental data become increasingly apparent, particularly within the shear layers at the interface between the cold jet and hot coflow. These deviations highlight the challenges of accurately capturing the complex interaction of turbulent mixing and scalar transport in regions where strong velocity gradients exist. These discrepancies are likely associated with the approximations made in determining the downstream position of the ODT line, as described in Eq. 8 and 9. While this approach is suitable for predicting centerline behavior, where downstream advection with an instantaneous bulk velocity is more appropriate, it appears to be less reliable for capturing the complex dynamics in regions with strong shear in radial direction.

This limitation highlights an important area where the current simulation procedure could be improved. Replacing the temporal ODT formulation with a spatial ODT approach, as proposed by Lignell et al. (2018), would explicitly account for the spatial variation of the velocity field in the radial direction. Such a formulation would allow the ODT line to advect more realistically downstream, improving predictions in shear-dominated regions and providing a more faithful representation of the complex interaction between turbulent mixing and chemical reaction. By capturing the lateral variations of the flow, this approach could more accurately represent the spatial distribution of temperature, mixture fraction, and their fluctuations throughout the flame, particularly in regions where strong radial shear strongly influences scalar transport.

Overall, the comparison between ODT and experimental measurements demonstrates that the ODT framework effectively captures the initial mixing processes and the general trends of the scalar fields. At the same time, the observed deviations in the shear-dominated regions underscore the influence of the advection mechanism on the local interplay between turbulence, mixing, and reaction. These findings emphasize both the strengths of ODT in representing mixing-dominated regions and the potential for further refinement to accurately resolve shear-driven effects in turbulent reacting flows.

4.3 Scatter plots

Figure 4 presents scatter plots of temperature versus mixture fraction and OH mole fraction versus mixture fraction at four downstream positions along the flow (z/D = 15,40,50,70). These plots represent the instantaneous values of the scalar fields at each computational grid cell for a fixed axial location, providing a detailed view of the local state of the reactive mixture. To

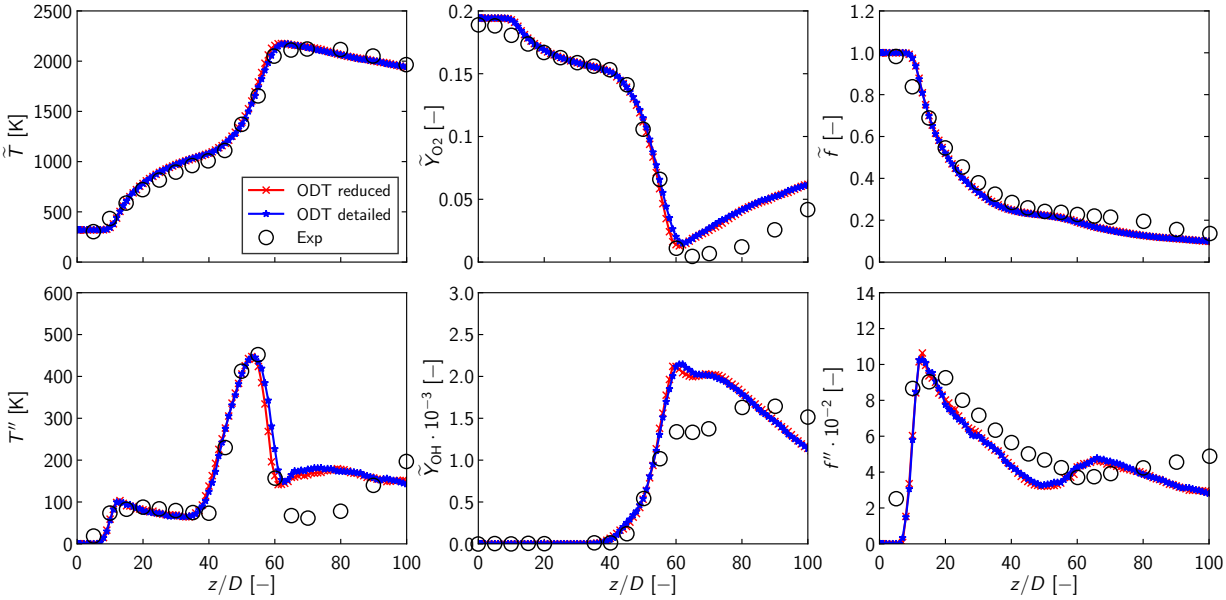

Fig. 2: Centerline profiles of Favre-averaged temperature ($\tilde{T}$ and fluctuations T''), species mass fractions (Favre-averaged oxygen mass fraction $\tilde{Y}_{O_2}$ and Favre-averaged hydroxyl radical mass fraction $\tilde{Y}_{OH}$), and mixture fraction ($\tilde{f}$ and fluctuations f'') from ODT simulations using a reduced and detailed reaction mechanism for the representation of the methane/air combustion. ODT results are compared to the experimental measurements of Cabra et al. (2005) (Exp).

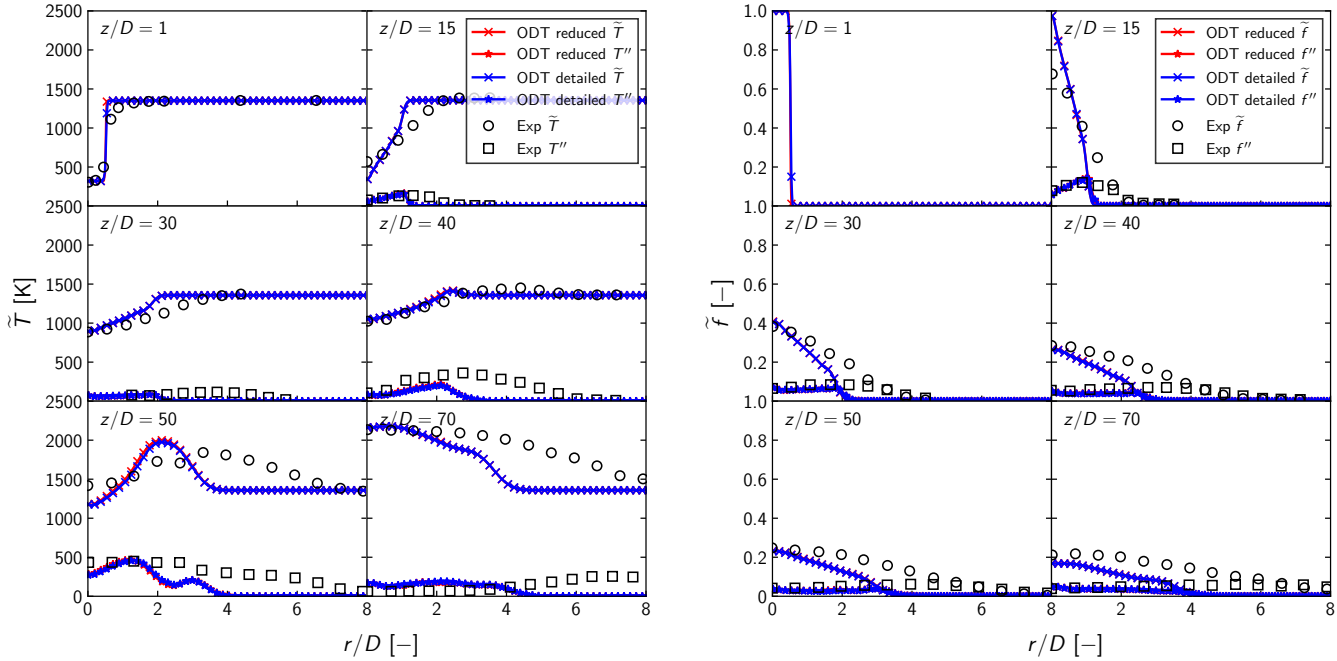

Fig. 3: Radial profiles of Favre-averaged temperature ($\tilde{T}$) and temperature fluctuations (T'') (left) and Favre-averaged mixture fraction ($\tilde{f}$) and mixture-fraction fluctuations (f'') (right) at downstream positions z/D = 1,15,30,40,50, and 70, obtained from ODT simulations using reduced and detailed reaction mechanisms for methane/air combustion. ODT results are compared with experimental measurements of Cabra et al. (2005) (Exp).

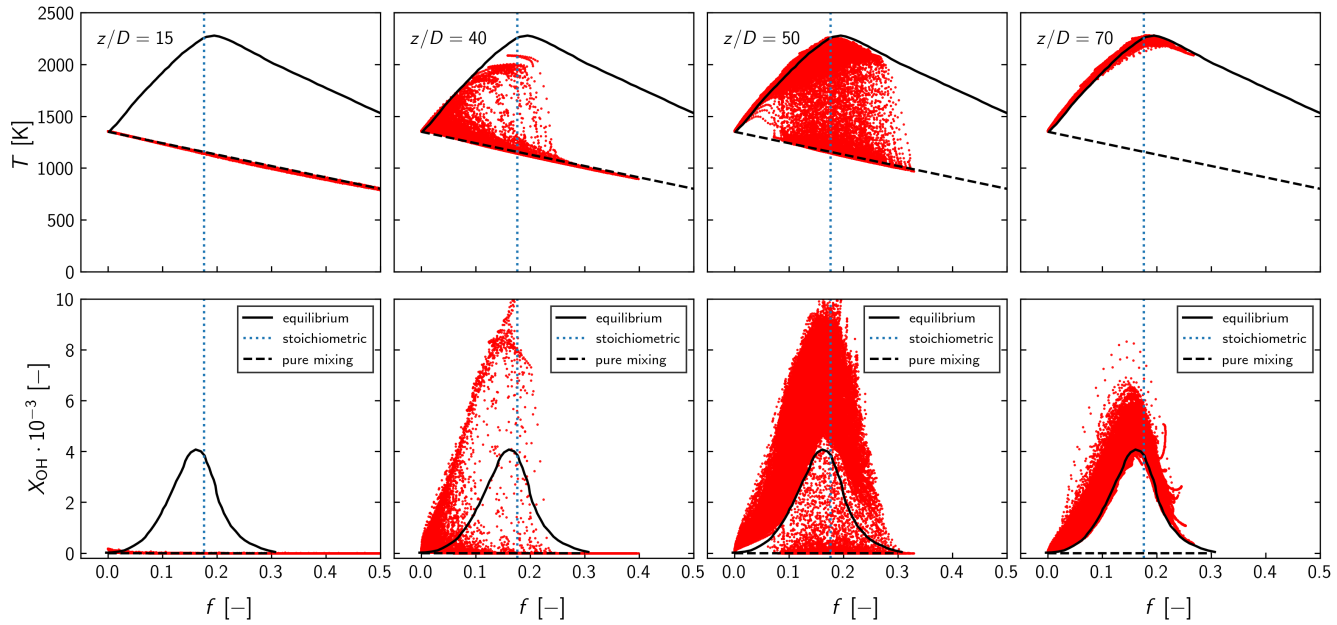

Fig. 4: Scatter plots at four different downstream positions (z/D = 15,40,50, and 70) from ODT simulations using the detailed reaction mechanism for methane/air combustion. The scatter plots are showing the instantaneous distribution of temperature versus mixture fraction and OH mole fraction versus mixture fraction.

improve readability, only 50 realizations from the full ensemble of 1500 simulations are displayed, offering a representative sample while avoiding excessive overlap of data points.

In each scatter plot, a vertical dotted line denotes the stoichiometric mixture fraction, $f_s = 0.17$, while a dashed line represents the non-reacting state corresponding to pure mixing without chemical reaction. The solid black line indicates the chemical equilibrium state. Together, these reference lines allow direct assessment of how local scalar values evolve from initial mixing toward chemical equilibrium along the flow.

At the upstream position z/D = 15, the scatter plots show that the flow is dominated by non-reactive mixing: temperature fluctuations are low, OH mole fractions remain near zero, and data points are distributed along the pure mixing line. This confirms that chemical reactions have not yet initiated and that the local state is governed primarily by turbulent mixing between the cold jet

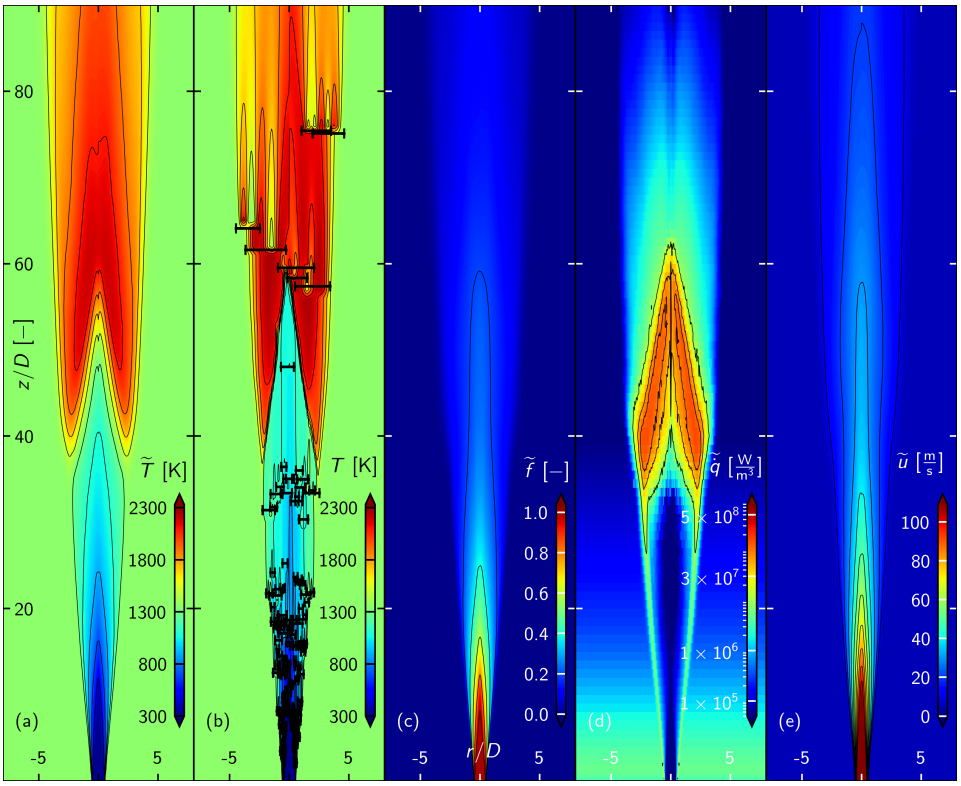

Fig. 5: Two-dimensional visualizations of the lifted methane/air jet flame from ODT simulations using the detailed reaction mechanism. Panels (a, c–e) show Favre-averaged fields: (a) temperature $\tilde{T}$, (c) mixture fraction $\tilde{f}$, (d) heat release rate $\tilde{q}$, and (e) downstream velocity $\tilde{u}$. These renderings illustrate the axial and radial evolution of the flame, capturing the initial mixing, flame stabilization, and the spatial structure of the reacting flow. Panel (b) shows the instantaneous temperature distribution from a single ODT realization, together with the positions of eddy events indicated by black bars. These eddy events represent the stochastic turbulent transport inherent to ODT, which models the effects of three-dimensional turbulence along the one-dimensional line.

and the hot coflow.

At intermediate positions $z/D = 40$ and $z/D = 50$, the scatter plots reveal a transitional behavior. Some data points have moved toward the equilibrium line, indicating regions where ignition and reaction have begun, while others remain near the pure mixing line. This spread illustrates the heterogeneous nature of flame development in the lifted jet, where turbulence and mixing create local pockets that react at different rates, reflecting the interplay between chemical kinetics and local scalar transport.

By $z/D = 70$, the majority of data points align along the equilibrium line, indicating that the system has reached near-complete chemical equilibrium. Temperature is maximized, and OH mole fractions reflect sustained combustion, demonstrating the establishment of a stabilized flame structure.

Overall, the scatter plots demonstrate that the ODT model successfully captures the key features of combustion, including the distribution of temperature and reactive species such as OH as a function of mixture fraction. They illustrate not only the progression from non-reactive mixing to ignition but also the establishment of a stabilized flame further downstream. Furthermore, the ODT results reproduce the qualitative and quantitative trends reported in the experimental measurements of Cabra et al. (2005) (not shown here), confirming ODT's ability to resolve the coupled effects of turbulence, mixing, and chemical reaction in a reduced-order framework.

4.4 Two-dimensional visualizations of the lifted jet flame

Figure 5 (a, c–e) presents two-dimensional renderings of the Favre-averaged temperature, mixture fraction, heat release rate, and downstream velocity, respectively. Although ODT is inherently a one-dimensional model, the generation of such two-dimensional visualizations of the lifted jet flame represents a notable and insightful achievement. These renderings demonstrate that, despite its reduced dimensionality, ODT is capable of capturing the essential spatial structure and dynamics of the turbulent reacting flow. They provide a complementary perspective to the previously discussed centerline and radial profiles, as well as the scatter plots of scalar quantities, allowing a more comprehensive understanding of the evolution of the flame and flow.

In Figure 5(b), the temperature field is shown together with the positions of eddy events from a single ODT realization, indicated by black bars. These eddy events represent the stochastic turbulent transport inherent to the ODT framework, which allows the model to incorporate effects of three-dimensional turbulence within a one-dimensional formulation. By visualizing these events, the figure provides insight into how turbulence intermittently enhances mixing and reaction along the flame.

Consistent with the centerline and radial profiles, the upstream region $z/D \lesssim 40$ is dominated by pure mixing between the cold jet and the hot coflow, resulting in a gradual temperature increase. At approximately $z/D \approx 45$, the flame enters the stabilization phase, marked by a sharp rise in temperature, rapid oxygen consumption, and a substantial increase in heat release. This indicates the onset of sustained combustion and the formation of a stable flame structure. Further downstream, the spatial distributions reveal the combined effects of turbulent mixing, scalar transport, and chemical reaction, emphasizing the ability of ODT to resolve the interplay between turbulence and chemistry along the axial direction.
Overall, these two-dimensional visualizations demonstrate that, despite its reduced dimensionality, ODT can provide a physically consistent and detailed depiction of flame evolution, highlighting both mean structures and the stochastic nature of turbulence-driven mixing.

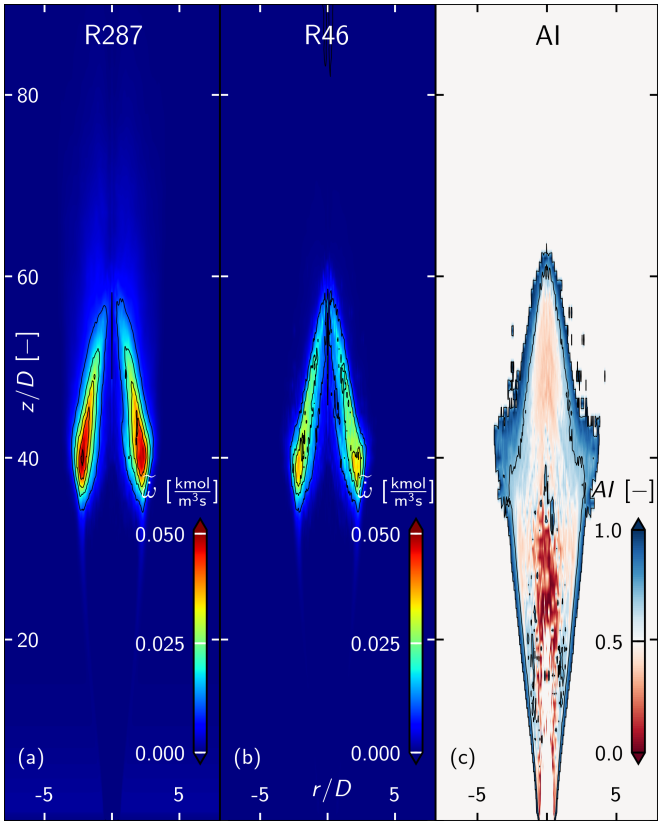

Fig. 6: Two-dimensional renderings illustrating the Favre-averaged net reaction rate of HO_2 associated with reaction 287 (a), Favre-averaged net reaction rate of HO_2 associated with reaction 46 (b), and corresponding mean autoignition index (AI) (c).

4.5 Autoignition index

The autoignition index (AI) provides a quantitative measure for distinguishing between autoignition- and propagation-driven reaction zones, as detailed in Schulz et al. (2017). Its definition is based on a comprehensive analysis of reaction rate fluxes within the HO_2 chemistry. In the detailed GRI-Mech 3.0 mechanism (Smith et al., 1999), which comprises 53 species and 325 reactions, HO_2 participates in numerous reaction pathways. Among these, the following two reactions have been identified as particularly influential in governing HO_2 consumption and, consequently, serve as key indicators for differentiating between autoignition- and propagation-dominated regions, in line with the investigations reported by Schulz et al. (2017).

$$\mathrm{HO_2 + H \longleftrightarrow OH + OH} \qquad \left[R46\right]$$

$$\mathrm{HO_2 + OH \longleftrightarrow H_2O + O_2} \qquad \left[R287\right]$$

By tracking these reactions, the AI effectively captures the transition from autoignition-driven to propagation-driven reaction behavior, highlighting the critical role of HO_2 in determining the combustion dynamics. In the reduced chemical mechanism, which consists of 19 species and a total of only 15 reactions, HO_2 is involved in only a single reaction equation. As a consequence, the evaluation of an AI index is not feasible at this stage, since the required contribution from multiple reactions controlling HO_2 consumption is not available.

The autoignition index is given by following definition (Schulz et al., 2017).

$$AI = \left| \frac{\dot{w}_{HO_2}^{R287}}{\dot{w}_{HO_2}^{R287} + \dot{w}_{HO_2}^{R46}} \right| \tag{11}$$

Here, $\dot{w}_{HO_2}^{R287}$ denotes the net reaction rate of HO_2 associated with reaction 287 in the detailed mechanism, whereas $\dot{w}_{HO_2}^{R46}$ represents the contribution of reaction 46 to the net HO_2 reaction rate. In the detailed GRI-Mech 3.0 mechanism, these two reactions play complementary roles in governing HO_2 chemistry: reaction 46 predominantly drives flame propagation, while reaction 287 is more closely linked to autoignition processes. Figure 6 shows two-dimensional renderings of the Favre-averaged net reaction rate of HO_2 for reaction 287 (a) and reaction 46 (b), highlighting the spatial regions where autoignition and propagation chemistry dominate, respectively. It can be observed that the highest values of $\dot{w}_{HO_2}^{R287}$ are reached in the range of $z/D \approx 35$ - 50, within the thin transitional region between the coflow and the flame. The highest values of $\dot{w}_{HO_2}^{R46}$ are observed in the range $z/D \approx 35$ to 45 and, compared to $\dot{w}_{HO_2}^{R287}$, are located closer to the flame core.

Figure 6 (c) presents the mean autoignition index, with blue regions ($AI > 0.5$) and red regions ($AI < 0.5$) corresponding to autoignition- and propagation-dominated reaction zones, respectively. In the flame, propagation is primarily concentrated in the core, while autoignition is dominant in the transitional region adjacent to the hot coflow. Comparison with instantaneous AI results from 3-D LES simulations reported by Schulz et al. (2017) (not shown here) demonstrates that the ODT model accurately reproduces the spatial distribution of both autoignition- and propagation-driven zones. Remarkably, despite the reduced-order nature of ODT, it is capable of resolving the detailed distribution of the autoignition index, providing physically meaningful insight into the interplay between local radical chemistry and flame dynamics. This capability, combined with the strong agreement with LES-based findings, underscores ODT's effectiveness as a computationally efficient tool for capturing key features of complex turbulent combustion processes.

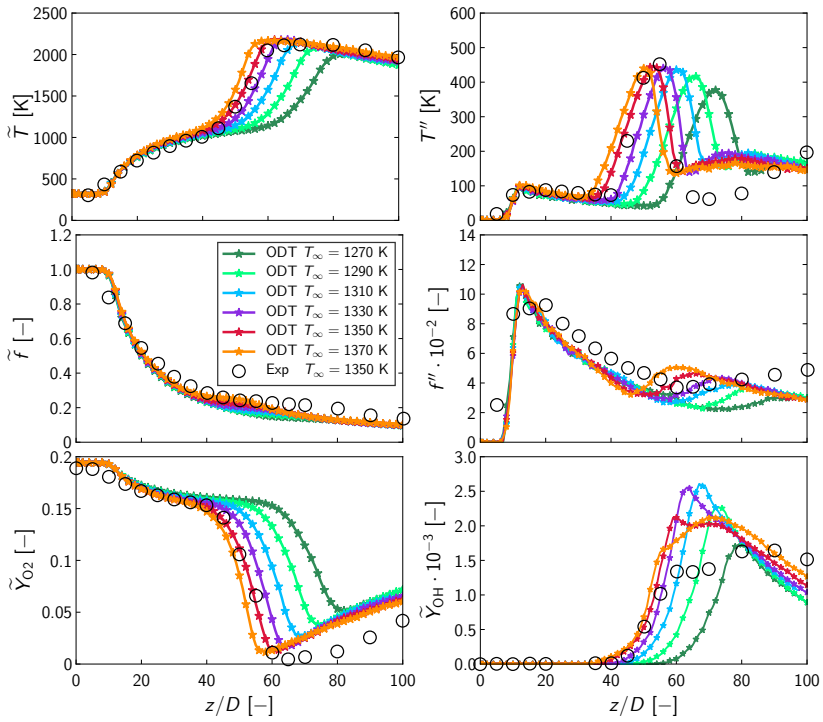

Fig. 7: Centerline profiles of Favre-averaged temperature ($\tilde{T}$ and fluctuations T''), mixture fraction ($\tilde{f}$ and fluctuations f''), and species mass fractions (Favre-averaged oxygen mass fraction $\tilde{Y}_{O_2}$ and Favre-averaged hydroxyl radical mass fraction $\tilde{Y}_{OH}$) obtained from ODT simulations using a reduced reaction mechanism (Lu and Law, 2008). The profiles illustrate the sensitivity of the methane/air flame to variations in the coflow temperature (1270 K, 1290 K, 1310 K, 1330 K, 1350 K, and 1370 K). For comparison, ODT results and corresponding experimental data (Cabra et al., 2005) (Exp) for the base case (1350 K) are also shown.

4.6 Liftoff height sensitivity

Figure 7 illustrates the sensitivity of jet combustion to variations in the coflow temperature. Shown are centerline profiles of the Favre-averaged temperature ($\tilde{T}$ and fluctuations T''), mixture fraction ($\tilde{f}$ and fluctuations f''), and species mass fractions (Favre-averaged oxygen mass fraction $\tilde{Y}_{O2}$ and Favre-averaged hydroxyl radical mass fraction $\tilde{Y}_{OH}$) for initial coflow temperatures of 1270 K, 1290 K, 1310 K, 1330 K, 1350 K, and 1370 K. The ODT results were obtained using the reduced mechanism of Lu and Law (2008), which closely reproduces the detailed mechanism, as shown for the base case in Figure 2, while substantially reducing computational cost and enabling more efficient simulations.

Decreasing the coflow temperature leads to a systematic downstream shift of the main heat-release region, indicating delayed combustion. This behavior is reflected by a later onset and a flatter rise of the centerline temperature, accompanied by more moderate oxygen consumption during the flame stabilization phase, relative to the base case at 1350 K. In contrast, increasing the coflow temperature promotes earlier ignition and stabilization, as evidenced by an upstream shift of the temperature rise and a more rapid depletion of oxygen.

An analogous trend is observed for variations in the jet velocity, as shown in Fig. 8 (a). Reducing the jet velocity to 80 m/s results in earlier flame stabilization and a steeper temperature increase compared with the base case at 100 m/s. For higher jet velocities (130, 150, 175, 200, and 250 m/s), combustion is progressively delayed, which manifests as a downstream shift of the temperature rise and reduced oxygen consumption in the stabilization region. This behavior is consistent with increased axial momentum and strain, which tend to inhibit early flame anchoring.

By contrast, variations in the coflow velocity have only a minor influence on the combustion characteristics, as shown in Fig. 8 (b). The centerline profiles corresponding to coflow velocities of 4.5, 5.0, 5.4, 6.0, and 6.5 m/s exhibit nearly identical behavior, indicating that, within the investigated range, changes in coflow velocity do not significantly affect flame stabilization or heat release.

Overall, these results are in good agreement with the parametric experimental measurements of Ref. Cabra et al. (2005), which report a strong sensitivity of flame liftoff height to variations in jet velocity and coflow temperature, and a comparatively weak dependence on coflow velocity.

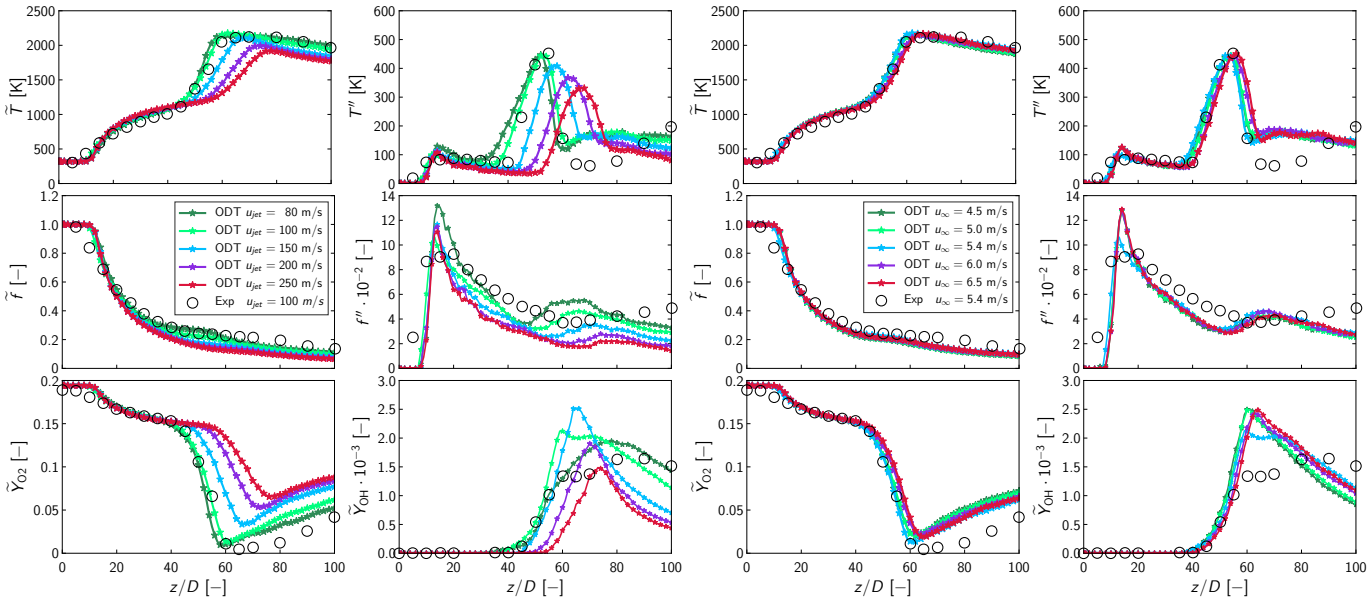

Fig. 8: Centerline profiles of Favre-averaged temperature ($\tilde{T}$ and fluctuations T''), mixture fraction ($\tilde{f}$ and fluctuations f''), and species mass fractions (Favre-averaged oxygen mass fraction $\tilde{Y}_{O_2}$ and Favre-averaged hydroxyl radical mass fraction $\tilde{Y}_{OH}$) obtained from ODT simulations using a reduced reaction mechanism (Lu and Law, 2008). The profiles illustrate the sensitivity of the methane/air flame to variations in the jet velocity (left side: 80 m/s, 100 m/s, 150 m/s, 175 m/s, 200 m/s) and coflow velocity (right side: 4.5 m/s, 5.0 m/s, 5.4 m/s, 6.0 m/s, and 6.5 m/s). For comparison, ODT results and corresponding experimental data (Cabra et al., 2005) (Exp) for the base case (100 m/s jet velocity and 5.4 m/s coflow velocity) are also shown.

5 Conclusions

In this study, ODT simulations of a lifted methane/air jet flame in a hot, vitiated coflow were carried out using a temporal ODT formulation, employing a detailed chemical mechanism (53 species, 325 reactions) and a reduced mechanism (19 species, 15 reactions). By applying downstream advection of the ODT line based on a continuously computed bulk velocity, the temporal evolution of the flame can be mapped to downstream spatial positions, enabling detailed analysis of the flame structure, species distributions, and reaction zones along the jet. The results were systematically compared to experimental measurements of Cabra et al. (2005), demonstrating that ODT can reasonably reproduce Favre-averaged centerline profiles of temperature, species mass fractions, and mixture fraction, as well as their fluctuations. Radial profiles in the initial mixing region ($z/D \lesssim 40$) also show good agreement, whereas deviations further downstream reveal the limitations of the applied downstream advection approach for the ODT line. At this stage, a spatial ODT formulation would be preferable, as it does not rely on the assumption of advecting the ODT line with a bulk velocity. Differences between the detailed and reduced mechanisms are negligible, confirming that the reduced mechanism, resulting from a stepwise simplification of the detailed GRI-Mech 3.0 mechanism, provides a computationally efficient approach while accurately capturing the key combustion features. Scatter plots further demonstrate that ODT captures the essential combustion characteristics and achieves reasonable agreement with experimental measurements. Two-dimensional visualizations of the lifted methane/air jet flame illustrate ODT's capability to provide spatially resolved information from a reduced-order simulation. Moreover, the efficiency of ODT enables computationally demanding parametric studies, such as the demonstrated

sensitivity to variations in coflow temperature, jet velocity, and coflow velocity, while also allowing the use of detailed chemical mechanisms required, for example, for the calculation of the autoignition index. Overall, the study shows that ODT is a reliable and efficient tool for investigating lifted methane/air jet flames in vitiated environments. Its ability to reproduce both global flame characteristics and detailed local statistics makes it well suited for parametric studies, sensitivity analyses, and the development of predictive models for reactive jet flames. The findings emphasize that reduced-order, scale-resolving models like ODT can bridge the gap between detailed simulations and experimental measurements, providing both physical insight and computational efficiency for complex turbulent combustion systems.

Acknowledgements

This research is supported by the German Federal Government, the Federal Ministry of Education and Research, and the State of Brandenburg within the framework of the joint project EIZ: Energy Innovation Center [project numbers 85056897 and 03SF0693A] with funds from the Structural Development Act (Strukturstärkungsgesetz) for coal-mining regions and the Brandenburg University of Technology (BTU) Graduate Research School [Conference Travel Grant].

References

W.T. Ashurst and A.R. Kerstein. One-dimensional turbulence: Variable-density formulation and application to mixing layers. *Physics of Fluids*, 17:025107, 2005. doi: 10.1063/1.1847413.

R.W. Bilger, S.H. Stårner, and R.J. Kee. On reduced mechanisms for methane-air combustion in nonpremixed flames. *Combustion and Flame*, 80:135–149, 1990. doi: https://doi.org/10.1016/0010-2180(90)90122-8.

R. Cabra, T. Myhrvold, J.-Y. Chen, R.W. Dibble, A.N. Karpetis, and R.S. Barlow. Simultaneous laser Raman-Rayleigh-LIF measurements and numerical modeling results of a lifted turbulent H2/N2 jet flame in a vitiated coflow. *Proceedings of the Combustion Institute*, 29:1881–1888, 2002. doi: https://doi.org/10.1016/S1540-7489(02)80228-0.

R. Cabra, J.-Y. Chen, R.W. Dibble, A.N. Karpetis, and R.S. Barlow. Lifted methane–air jet flames in a vitiated coflow. *Combustion and Flame*, 143(4):491–506, 2005. ISSN 0010-2180. doi: https://doi.org/10.1016/j.combustflame.2005.08.019.

P. Domingo and L. Vervisch. Recent developments in DNS of turbulent combustion. *Proceedings of the Combustion Institute*, 39: 2055–2076, 2023. doi: https://doi.org/10.1016/j.proci.2022.06.030.

P. Domingo, L. Vervisch, and D. Veynante. Large-eddy simulation of a lifted methane jet flame in a vitiated coflow. *Combustion and Flame*, 152:415–432, 2008. doi: https://doi.org/10.1016/j.combustflame.2007.09.002.

T. Echekki, A.R. Kerstein, and T. Dreeben. One-dimensional turbulence simulation of turbulent jet diffusion flames: model formulation and illustrative applications. *Combustion and Flame*, 125(3):1083–1105, 2001. doi: https://doi.org/10.1016/S0010-2180(01)00228-0.

K. Gkagkas and R.P. Lindstedt. Transported PDF modelling with detailed chemistry of pre- and auto-ignition in CH4/air mixtures. *Proceedings of the Combustion Institute*, 31:1559–1566, 2007. doi: https://doi.org/10.1016/j.proci.2006.08.078.

D. Goodwin. *Cantera C++ User's Guide*. California Institute of Technology, 2002.

R.L. Gordon, A.R. Masri, S.B. Pope, and G.M. Goldin. A numerical study of auto-ignition in turbulent lifted flames issuing into a vitiated co-flow. *Combustion Theory and Modelling*, 11(3):351–376, 2007. doi: 10.1080/13647830600903472.

M. Ihme and Y.C. See. Prediction of autoignition in a lifted methane/air flame using an unsteady flamelet/progress variable model. *Combustion and Flame*, 157:1850–1862, 2010. doi: https://doi.org/10.1016/j.combustflame.2010.07.015.

A.R. Kerstein. A linear eddy model of turbulent scalar transport and mixing. *Combustion Science and Technology*, 60:391–421, 1988. doi: 10.1080/00102208808923995.

A.R. Kerstein. Linear-eddy modeling of turbulent transport. Part 3. Mixing and differential molecular diffusion in round jets. *Journal of Fluid Mechanics*, 216:411–435, 1990. doi: 10.1017/S0022112090000489.

A.R. Kerstein. Linear-eddy modelling of turbulent transport. Part 7. Finite-rate chemistry and multi-stream mixing. *Journal of Fluid Mechanics*, 240:289–313, 1992. doi: 10.1017/S0022112092000107.

A.R. Kerstein. One-dimensional turbulence: model formulation and application to homogeneous turbulence, shear flows, and buoyant stratified flows. *Journal of Fluid Mechanics*, 392:277–334, 1999. doi: 10.1017/S0022112099005376.

T. Lackmann, A.R. Kerstein, and M. Oevermann. A representative linear eddy model for simulating spray combustion in engines (RILEM). *Combustion and Flame*, 193:1–15, 2018. ISSN 0010-2180. doi: 10.1016/j.combustflame.2018.02.008.

D.O. Lignell, A.R. Kerstein, G. Sun, and E.I. Monson. Mesh adaption for efficient multiscale implementation of one-dimensional turbulence. *Theoretical and Computational Fluid Dynamics*, 27(3-4):273–295, apr 2013. doi: 10.1007/s00162-012-0267-9.

D.O. Lignell, V. Lansinger, Juan A. Medina M., M. Klein, A.R. Kerstein, H. Schmidt, M. Fistler, and M. Oevermann. One-dimensional turbulence modeling for cylindrical and spherical flows: model formulation and application. *Theoretical and Computational Fluid Dynamics*, 32:495–520, 2018. doi: 10.1007/s00162-018-0465-1.

T.F. Lu and C.K. Law. A criterion based on computational singular perturbation for the identification of quasi steady state species: A reduced mechanism for methane oxidation with NO chemistry. *Combustion and Flame*, 154:761–774, 2008. doi: https://doi.org/10.1016/j.combustflame.2008.04.025.

R. McDermott. *Towards one-dimensional turbulence subgrid closure for large-eddy simulation*. PhD thesis, University of Utah, 2005.

J.A. Medina M., H. Schmidt, F. Mauss, and Z. Jozefik. Constant volume n-heptane autoignition using One-Dimensional Turbulence. *Combustion and Flame*, 190:388–401, January 2018. doi: https://doi.org/10.1016/j.combustflame.2017.12.015.

J.-B. Michel, O. Colin, C. Angelberger, and D. Veynante. Using the tabulated diffusion flamelet model adf-pcm to simulate a lifted methane–air jet flame. *Combustion and Flame*, 156:1318–1331, 2009. doi: https://doi.org/10.1016/j.combustflame.2008.12.012.

M. Oevermann, H. Schmidt, and A.R. Kerstein. Investigation of autoignition under thermal stratification using linear eddy modeling. *Combustion and Flame*, 155:370–379, 2008. doi: https://doi.org/10.1016/j.combustflame.2008.04.020.

S.B. Pope. PDF methods for turbulent reactive flows. *Progress in Energy and Combustion Science*, 11:119–192, 1985. doi: 10.1016/0360-1285(85)90002-4.

A. Ricks, J. Hewson, A.R. Kerstein, J. Gore, S. Tieszen, and W.T. Ashurst. A spatially developing one-dimensional turbulence (ODT) study of soot and enthalpy evolution in meter-scale buoyant turbulent flames. *Combustion Science and Technology*, 182: 60–101, 2010. doi: 10.1080/00102200903297003.

S. Sannan, T. Weydahl, and A.R. Kerstein. Stochastic simulation of scalar mixing capturing unsteadiness and small-scale structure based on mean-flow properties. *Flow, Turbulence and Combustion*, 90:189–216, 2013. doi: 10.1007/s10494-012-9436-6.

O. Schulz, T. Jaravel, T. Poinsot, B. Cuenot, and N. Noiray. A criterion to distinguish autoignition and propagation applied to a lifted methane–air jet flame. *Proceedings of the Combustion Institute*, 36:1637–1644, 2017. doi: https://doi.org/10.1016/j.proci.2016.08.022.

S. Sharma, M. Klein, and H. Schmidt. Features of far-downstream asymptotic velocity fluctuations in a round jet: A one-dimensional turbulence study. *Physics of Fluids*, 34:085134, 2022. doi: 10.1063/5.0101270.

G.P. Smith, D.M. Golden, M. Frenklach, N.W. Moriarty, B. Eiteneer, M. Goldenberg, C.T. Bowman, R.K. Hanson, S. Song, W.C. Gardiner, V.V. Lissianski, and Z. Qin. http://www.me.berkeley.edu/gri_mech/. *Technical report*, 1999.

H. Zhang, Z. Yu, T. Ye, M. Zhao, and M. Cheng. Large eddy simulation of turbulent lifted flame in a hot vitiated coflow using tabulated detailed chemistry. *Applied Thermal Engineering*, 128:1660–1672, 2018. ISSN 1359-4311. doi: https://doi.org/10.1016/j.applthermaleng.2017.09.110.